POLITECNICO
MILANO 1863

DIPARTIMENTO DI MECCANICA

mecc

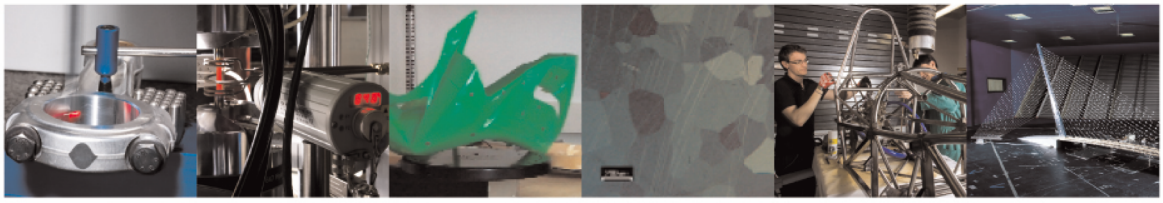

Application of shot peening to case-hardened steel gears: the effect of gradient material properties and component geometry

Heydari Astaraee A.;Bagherifard S.;Bradanini A.;Duo P.;Henze S.;Taylor B.;Guagliano M.

This is a post-peer-review, pre-copyedit version of an article published in Surface and Coatings Technology. The final authenticated version is available online at:
https://doi.org/10.1016/j.surfcoat.2020.126084

© <2020>

This content is provided under CC BY-NC-ND 4.0 license

DIPARTIMENTO DI MECCANICA ■ POLITECNICO DI MILANO
via G. La Masa, 1 ■ 20156 Milano ■ EMAIL (PEC): pecmecc@cert.polimi.it
http://www.mecc.polimi.it
Rev. 0

Application of shot peening to case-hardened steel gears: numerical and experimental investigation on the effect of gradient material properties and component geometry

Asghar Heydari Astaraee[1], Sara Bagherifard[1], Andrea Bradanini[1], Pierangelo Duó[2], Steffen Henze[3], Benjamin Taylor[3], Mario Guagliano[1]

[1]Department of Mechanical Engineering, Politecnico di Milano, 20156 Milan, Italy

[2]Rolls-Royce Deutschland Ltd & Co KG, Eschenweg 11, Dahlewitz, 15827 Blankenfelde-Mahlow, Germany

[3]Aerospace Transmission Technologies GmbH, Adelheidstraße 40, 88046 Friedrichshafen, Germany

Abstract

Shot peening is a mechanical surface treatment widely utilized to enhance the fatigue strength of gears by surface work hardening and inducing compressive residual stresses while also altering the surface roughness. This study is aimed at developing a detailed numerical model of dual shot peening on case hardened gears by considering the variation of material properties through the thickness. Two different approaches were implemented to estimate the gradient material properties of case-hardened steel. In the first approach, empirical relations were used to adjust the flow stress to the local hardness variation through the thickness. In the latter approach, a set of experimental tests and finite element modeling of an indentation were utilized to obtain the stress-strain response of the gradient structure using inverse analysis. The intricate geometry of the gear also necessitated simulating the shot kinetics on the gear tooth using appropriate impact angles. Various modeling approaches were incorporated to consider the deviation of the impact angle due to geometrical features. The results indicate that a local 3D cubic cell model can be successfully implemented to predict the final distribution of residual stresses and surface roughness. The results are critically discussed in terms of the applied modeling approaches.

Keywords: finite element analysis, shot peening, carburization, inverse analysis

1. Introduction

Gears of high-power density transmission systems are mostly made of case-hardened steels. Due to the hardened case and the compressive residual stresses induced within it, case-hardened gears are highly resistant to wear, bending fatigue and contact fatigue. Recently the developed technologies for power transmission systems aimed at increasing torque and power density have put a limiting factor on the lifetime of involved gears. Thus, investigations on the application of shot peening (SP) to manufactured gears have attracted further attention.

Owing to the service conditions, gears are both prone to bending fatigue at the root of the tooth and rolling contact fatigue along the tooth flank and SP has proven to be beneficial to both types of damage. Widmark and Melander [1] reported the contact fatigue tests on case-hardened steels with various sequences of grinding, case-hardening treatment, and SP. Their results showed that SP rendered the highest resistance to contact fatigue. Benedetti et al. [2] combined SP with case-hardening treatment to investigate the effects on the fatigue behavior of spur gears. They discussed the results by building up a simple numerical model to estimate the stresses at the gear tooth root and predict fatigue crack initiation. The combined case-hardening and SP treatments showed an advantageous effect on fatigue life/resistance by expanding the compressive residual stresses to deeper regions. Guagliano et al. [3] studied the contact fatigue damage in carburized gears followed by SP treatment. They suggested an approach for the evaluation of SP parameters on fatigue performance by implementing a numerical model. The proposed approach enabled the optimization of parameters for fatigue endurace enhancement. Further to fatigue-related improvements, SP could be employed in the manufacturing of carburized gears to increase the durability against pitting, to compensate the tensile residual stresses induced by machining, to enhance lubrication, and also to eliminate the stress risers caused by machining [4].

The ability to numerically model the SP process and predict the final surface state in terms of topography and induced stresses is of utmost interest; it can facilitate correlating the effect of process parameters to the performance of the treated part. There are numerous processing parameters involved, thus experimental investigations can be time-consuming and economically less favorable, especially from an industrial point of view. The modeling procedure is very complex as SP is a dynamic highly non-linear problem in which multiple subsequent impacts take place. In recent years, there have been significant advancements in numerical modeling of the SP process.

In the developed numerical models so far in the literature, different approaches have been used for the incorporation of SP coverage into multiple impact models. Early models contained prepositioned shots in which the shot sequences, as well as their positions, were predetermined. Meguid et al. [5] constructed a 3D finite element model that consisted of a quarter of a cube considering the symmetry with a twin shot impacting the metallic target. They discussed the effects of shot velocity, size, shape, and separation distance on the induced deformations and stress field. Al-Hassani et al. [6] created a model consisting of five-shot successive series with overlaps along the diagonal of the target impacting the surface in a normal direction. Guagliano [7] used a circular pattern to position the five shots: three at the vertices of a quarter of a circle and one in the middle of circle arc. The fifth shot was the repetition of the initial one. Kang et al. [8] developed a more sophisticated model regarding the coverage by the implementation of a MATLAB program to create a series of impacts with uniform distribution in space and time. Another common model within this category is the symmetry cell (with the application of symmetric boundary conditions on all side faces of the target), which is computationally cost-effective [9]. However, as it can be deduced, predetermined models do not consider the random nature of shot impingement during the SP process. It has been shown that full coverage conditions cannot be met with prepositioned models [10]. In this regard, more realistic random

positioned models were purposed in terms of both impingement location and sequence. A function was utilized to randomly generate the coordinates of the impacting shots [11]. The model was upgraded afterward [12], incorporating the Avrami model with 100% coverage evolution formulated by Kirk and Abyaneh [13]. It has been shown that a random position generator function could be handled to have the numerical coverage evolution fully match with the experimental one [14]. Numerous investigations have been performed on the modeling details such as mesh sensitivity [12], initial surface finish [15], and material constitutive model [16]. However, to the best of the authors' knowledge, there exists a very limited number of studies on the modeling of SP applied to carburized steels, both for the complexity of the gear geometry and the intricacy of the gradient properties induced by case-hardening. The most detailed one was performed by Donzella et al. [17], who developed a numerical simulation on the effects of SP on carburized 16MnCr5 steel in terms of residual stress distribution. A multiple impact model with prepositioned shots was developed as it was mentioned that the determination of the optimum sequence of shots needed more investigations. A sequence of shots that led to a stabilized residual stress profile in a flat target model after a certain number of impacts was used to examine different combinations of shot size and velocity, and various case depths. The model was used to identify the optimum combination of parameters for maximum residual stresses; however, the proposed model was not experimentally validated [17].

More than a decade has passed from the introduction of random multiple impact models proposed for the prediction of air blast SP process effects. Nevertheless, their application to industry scale gears with geometrical and materialistic complexities has not been studied extensively. Gears are usually made of case-hardened steel, consist of several tens of teeth around the edge, and are commonly shot peened by being rotated under shot stream using air blast SP process. Thus, the implementation of numerical modeling of the SP process regarding

case-hardened gears requires further model improvements, regarding its particular material and geometrical aspects.

Herein, we selected a carburized aeronautic gear that is shot peened at the final stage of the manufacturing process. We show that the dual SP process results in terms of residual stresses and surface roughness can be estimated with acceptable precision elaborating the existing random multiple impact models through implementing both material gradient and geometrical complexities. The stress-strain response of the gradient case-hardened gear was anticipated using two approaches, namely hardness-based, and inverse analysis approach. In the former approach, the microhardness profile of the case-hardened gear was implemented for stress-strain calculations. In the latter approach, inverse analysis, a more complex method, was applied to obtain the stress-strain response of the carburized layer using numerical simulation of a spherical indentation test validated by an experimental procedure. The detailed gear geometry was suggested to be considered implicitly by assigning appropriate impact angles using either fixed mean impact angle or varying impact angles based on the relative direction of the shot stream with respect to the tooth geometry as the gear is rotated. The induced residual stresses and final surface roughness obtained following the proposed models showed very good agreement with the experimental data.

2. Numerical modeling

2.1. Material model

Gear material is carburizing steel, the grade of which is the courtesy of Aerospace Transmission Technologies GmbH and is subject to confidentiality. The gear undergoes a carburization heat treatment with a final core microstructure of tempered martensite and tempered bainite, and a case microstructure of fine and tempered martensite with no visible retained austenite. The stress-strain curve characteristic of the core material normalized by the ultimate tensile strength of the material is shown in Fig. 1.

The material model considered for the carburized steel consists of elastic and plastic properties. The stress-strain curve for a carburized steel is variable over the case region based on the gradient carbon content. Depending on global parameters of the SP process i.e. coverage and intensity, the induced plastic deformation can be extended to a certain fraction of the case-hardened layer. Since SP is a process with local plastic deformation mainly focused on the surface region, the characterization of the plastic flow behavior on the surface and within the case is of utmost importance for successful SP simulations. In the current research, two approaches were considered to characterize the plastic flow of the case. The first approach, hereafter called hardness-based approach, is basically estimating the material properties of the core to the case, based on the local microhardness value. The second approach applies an inverse analysis to capture the material properties of the gradient structure inversely by modifying the material input for the simulation of an experimental indentation test. A review of the relevant literature showed that inverse analysis is one of the most well-known but yet challenging methods to calculate the stress-strain response of case-hardened materials. In the following sections, each of the approaches mentioned above is explained in detail.

2.1.1. Hardness-based approach

In this approach, an empirical equation [17] is used to locally calculate the yield stress of the carburized steel as a function of its Vickers microhardness throughout the case:

$$\sigma_y = -0.0016\,HV^2 + 3.86\,HV - 222\ \ [MPa] \qquad (1)$$

This equation is suggested to be able to estimate the yield stress of hardened steel with a microstructure consisting of at least 90% Martensite [18]. From metallurgy, it is well known that the hardness of a martensitic structure is mainly dependent on the carbon content. Thus,

the variation in the hardness of the case in a carburized steel with a nearly martensitic structure is dominated by the carbon gradient stemming from the carburization process. The yield stress of the gear core material based on Eq. (1) is calculated to be approximately identical to the experimental yield stress (2.5% difference). This indicates that Eq. (1) is able to predict the yield stress of the core material with acceptable accuracy and can be used with confidence for the prediction of the yield stress of the case material. To define the plastic flow behavior of the case material, single yield stress as a function of depth is not sufficient, since strain hardening almost always occurs upon plastic deformation. To estimate the strain hardening behavior of the case material, the same hardening behavior was adopted for both the core and the case material, as suggested by Donzella et al. [17].

The Vickers microhardness of the carburized steel normalized with respect to the mean hardness of the case in the flank region of the gear is shown in Fig. 2a. To facilitate the numerical modeling, it was assumed that the carburized steel can be modeled with a stack of 10 layers; 9 layers for the case, denoted by L1-L9 and the last one for the core, as shown in Fig. 2b. The thickness of L1 is equal to the depth of constant hardness region immediately below the surface extracted from the experimental data, indicated by l_1. The rest of the case (equal to l_2) is divided into 8 intermediate layers (L2-L9) with equal thicknesses. An average hardness value was considered over any individual layer for the calculation of yield stress based on Eq. (1). This average value was calculated using a fitted linear function to the continuously decreasing part of the hardness profile indicated by l_2. It was assumed that this value is able to characterize the mean mechanical properties of the individual layers.

2.1.2. Inverse analysis approach

Inverse analysis stands for a method in which minimization of difference is performed directly between experimental data from a test e.g., indentation testing, and finite element simulations of the same test to find the material properties. It is called “inverse” since one tries to obtain

material properties (output) from a simulation, contrary to the usual case of forward analysis in which material properties are the input of the simulation. To perform the inverse analysis, a material constitutive law should be chosen, and the calculated results are based on the material constitutive parameters; then, upon the optimization, the main parameters are identified. The constitutive law for this set of analyses was selected to be Hollomon law for the elastic-plastic response of the carburized material:

$$\begin{cases} \sigma = E\varepsilon, & \sigma < \sigma_0 \\ \sigma = E^n \sigma_0^{1-n} \varepsilon^n, & \sigma > \sigma_0 \end{cases} \quad (2)$$

where E is Young's modulus, σ_0 is yield stress (equivalent to elastic limit), n is hardening exponent, and ε is the total strain. The experimental test used for the analysis was indentation testing with a spherical indenter, which is explained in detail in the following subsection. The experimental data are the load-displacement response recorded during the test. For the minimization purposes, least-squares minimization function was used as follows:

$$L(x) = \frac{1}{j}\sum_i^j [F_i^{Num}(x) - F_i^{Exp}]^2 \quad (3)$$

where $L(x)$ is the objective function for minimization, x is the vector of material parameters to be optimized (i.e. σ_0 and n), j is the total number of points, and $F_i^{Num}(x)$ and F_i^{Exp} are respectively, the numerical and experimental loads at each point i. The optimization problem was coded and solved using a MATLAB subroutine.

The inverse analysis started by performing two instrumented indentation tests one at the topmost hardened surface and the other at the core. The inverse analysis was followed to calculate the constitutive law parameters (i.e. σ_0 and n) for the core as a homogeneous material.

For the carburized steel, the hardness within the case was approximated by a bilinear behavior, as shown in Fig. 2a. Along with this assumption, the elastic-plastic constitutive behavior was considered to be estimated linearly within the case, as suggested by Moussa et al. [19, 20]:

$$\begin{cases} \sigma = \sigma_{ts}, & x < l_1 \\ \sigma = \sigma_{core} + \dfrac{\sigma_{ts} - \sigma_{core}}{l_2}(l_1 + l_2 - x), & l_1 < x < l_1 + l_2 \\ \sigma = \sigma_{core}, & x > l_1 + l_2 \end{cases} \quad (4)$$

Where σ_{ts}, σ_{core}, l_1 and l_2 are the flow stress for the topmost surface, the flow stress of substrate, the thickness of the uppermost surface layer, and intermediate layers, respectively, and x is the distance from the surface. The inverse analysis, along with Eq. (4) was followed to calculate the constitutive parameters of the surface layer using the 10-layer structure.

2.1.2.1. Indentation testing

A 10 mm diameter spherical indenter made of tungsten carbide was used for indentation tests. In order to record the load-displacement data during the tests, a conventional hydraulic tensile testing machine was used. To perform the test, a support made of 39NiCrMo3 steel for the indenter was designed such that the indenter could be fixed in place by a screw mechanism. The displacement was measured with a deflectometer the tip of which was in contact with the bottom face of the support while the load was recorded by the machine load cell. The experimental set-up is shown Fig. 3. The indentation experiments were repeated three times and performed in displacement control mode with a crosshead velocity of 0.12 mm/min.

2.1.2.2. Finite element model of the indentation test

The finite element model of the indentation tests consisted of a 2D axisymmetric model, as shown in Fig. 4a. ABAQUS Standard 2019, with a static general procedure, was incorporated. The ball indenter was modeled by a quarter of a circle with a diameter matching the experimental one (10 mm), Young's modulus of 670 GPa, and Poisson's ratio of 0.2. The steel

specimen was modeled by a half rectangle with dimensions of 13×15 mm^2, sufficiently large to remove the effects of boundaries. The plastic material properties of the specimen were calculated and input by the Matlab code in each optimization loop. Displacements of specimen bottom edge were fully fixed. The loading was accomplished by imposing a vertical displacement in the center of the ball while the horizontal displacement was restrained. Contact between the ball and specimen was defined by introducing a penalty contact method. Preliminary analyses showed that the load-displacement response is not sensitive to the coefficient magnitude ranging from 0.05 to 0.3. Therefore a friction coefficient of 0.1 was selected to reduce the contact nonlinearity. Both the ball and specimen were meshed using CAX4 linear elements. To increase the accuracy of modeling, the mesh in the contact region was refined. A mesh convergence study was performed and finally, a mesh size of 10 μm was used in the refined regions.

2.2. 3D multi-impacting model of SP

3D modeling and simulation were conducted using finite element code ABAQUS Explicit 2019 for the development of the single impact and multiple impact models. The model comprised of a 3D cubic cell as the specimen and a 3D sphere as the shot, details of which are depicted in Fig. 4b. The dimensions of the cubic cell model were 3×3×3 mm^3 based on the authors' previous studies [21]. A circular impact area with a radius of 0.75 mm in the center of the cubic model was considered. The applied SP process was air-blast in which a stream of flying shots is accelerated by compressed air. The nozzle was placed within a 250 mm stand-off distance from the gear, as shown in Fig. 5. Two subsequent SP processes with the parameters displayed in Table I were applied to the gear. Owing to the purpose of the simulations, which is the assessment of residual stresses and surface roughness on specific locations of a gear tooth, it is deduced that a 3D cubic cell model proposed as in Fig. 4b could be used with some elaborations about the kinetics of impacts regarding the gear tooth geometry. This seems to be valid because

the modeling approach of SP introduced here is already a local one, which could be applied to any complicated geometry, as long as the impact direction encompasses geometrical features. In particular, regarding the residual stresses and surface roughness, the experimental measurements are often captured from an area equal to several square millimeters; thus, extra-large models may not necessarily be constructive concerning the accuracy of the simulations. For the particular case of gear, it should be stated that although the gear tooth has a very complicated geometry with curved surfaces, they could be considered as flat surfaces over the small distances, as long as the real impact angles induced by the relative direction of the shot stream and the macro-features of the gear tooth geometry are adapted. Specifically, regarding the flank region, which is mostly desired in the current study, and considering the size of the impact area in the numerical model, this assumption would be acceptable.

C3D8R elements (linear 8 nodes hexahedral with reduced integration) were used for meshing the model. To guarantee the elimination of residual oscillations, half infinite elements with a thickness of 1 mm were used in the side faces as well as the bottom face of the cube, as depicted in Fig. 4b. Half infinite elements offer silent boundaries by reducing the reflection of dilatational and shear waves back into the model. Mesh convergence study was performed using single impact analysis to remove the dependence of residual stress on the size of the element. Hence, a mesh size of $0.02\times0.02\times0.02$ mm^3 in the impact area was selected. The shot was meshed with a C3D8R element type with a smallest element size of 0.01 mm in the contact zone. The mesh details are shown in Fig. 4c. However, for the single impact analysis, much smaller mesh size in the impact area, as well as the shot (0.005 mm), was utilized to capture the indent size accurately.

The shot material for stages 1 and 2 of SP were ceramic media, with a radius of 0.72 mm and 1.0 mm, respectively. A friction coefficient equal to 0.2 was used considering a general contact algorithm [22]. To minimize element distortion under the severe deformations induced by shot

impact, Arbitrary Lagrangian-Eulerian (ALE) meshing technique in Abaqus was adapted. The stress-strain curve calculated by either the hardness-based method or the inverse analysis for each layer in Fig. 2b was assigned as input material properties of the carburized target model both for single and multiple impact SP simulations.

Regarding minimal temperature rises during SP, thermal effects were ignored in the analyses. The velocity was assigned to all nodes of the shot as an initial boundary condition. Residual stresses from the carburization heat treatment were introduced as pre-stresses into the model using the SIGINI subroutine, and a static general analysis was run to ensure the equilibrium state of the applied stresses.

Multiple-impact model of SP was constructed using Python scripting. A script was developed to create an individual model for each impact. Thus, any impact was accomplished by a separate analysis. In this regard, the results of the previous analysis was imported and assigned as initial conditions of the current impact. This strategy reduces the computational cost due to simultaneous presence of a large number of shots in the model. Shot impingement in SP, in terms of space and time, is random in nature. The impact sequence in multiple-impact model was, therefore, adapted to be random. Setting a random position to the shot, the initial conditions, and analysis control were conducted using a script.

Coverage evolution in air blast SP can be modelled by Avrami function. Thus, the total shot number to reach the full coverage level (98%) could be estimated using Avrami function [21]:

$$C = 100\{1 - \exp(-A_r)\} \quad (5)$$

$$A_r = N(\frac{d}{D})^2 \quad (6)$$

where A_r is indent ratio indicating the ratio of overall indent area to impact area, N is the shot number, d is indent size produced by a single impact and D is the diameter of the impact area.

To achieve full coverage (i.e. $C = 98\%$), a value of A_r equal to 3.91 should be met, which is fulfilled by the required total number of impacts. Indent size (d) was derived from the single impact simulation.

Shot kinetics during SP of the gear is important to extract the angle of shot impact and realistically reproduce the interaction of the shots and the gear tooth. It is emphasized that shot kinetics are most desired in the flank region, so the calculations of impact angle would be performed at the center of the flank. Details of the shot stream are shown in Fig. 5a. The stream consisted of three zones: (1) total spray zone, (2) full coverage zone, and (3) constant intensity zone. Fig. 5b reproduces the last zone of the stream on the gear. Among the three zones, the constant intensity zone was considered to be the most effective in terms of shot kinetics. This is because the velocity of the flying shots, which is a main governing factor for kinetic energy, is only guaranteed over the constant intensity zone. Thus, the measured shot velocity with respect to a certain intensity is solely valid over this zone, as the intensity would be lower out of the aforementioned zone. The maximum possible impact angle of the shot at the flank center was estimated to be ~35° considering all the possible placements of the gear in front of the shot stream (Fig. 5b). As the gear rotates in front of the stream, the angle of impact would change. Assuming a clockwise rotation, it could be deduced that the impact angle would decrease up to a situation where the direction of a flying shot is almost parallel to the surface of the flank center. This later stage dictates an impact angle of zero. Thus, it is postulated that the range of impact angle over the constant intensity zone is 0°-35°. With the rotation of the gear under the stream, this angle range is repeated during SP.

Several approaches come to the mind to consider the variation of impact angle. A more straightforward method for the shot kinetics would be to use the mean value of the impact angle, i.e., 17.5°, assigned to all shots. In this case, it was assumed that the average behavior of shot kinetics was considered. In more realistic approaches, varying impact angles with step

sizes of 12.5 and 5 were considered for the variation of the impact direction between successive shots. The impact angle was dictated by defining the components of velocity V_x and V_y considering the impact angle θ. Smaller step sizes than 5 were not incorporated due to the very high computational cost of small-angle impacts and their expected minor influence on the distribution of residual stresses. The initial impact started from the largest angle and decreased to the smallest one with the relevant step size. Then, the angle variation was repeated in a loop to mimic the gear rotation under the stream.

In the dual peening process, the second stage of SP was applied after the first stage with its particular process parameters, including media type and intensity, as described in Table I. In this regard, the same 3D cell model developed for the first stage SP was used for the second stage with the following considerations:

- Shot characteristics were changed to the relevant media;
- The final results of structural modeling for the first SP stage including displacements, strains, and stresses were imported as initial conditions for the 2^{nd} SP stage model;
- Coverage calculations, including the number of required impacts for full coverage were repeated for the 2^{nd} stage, based on the size of the indent made by a single impact on the not peened sample.

Roughness calculations were performed using a prepared Matlab subroutine. The initial coordinates of the nodes on the impact area as well as their final vertical displacements were extracted from the simulations and imported into the subroutine. The subroutine was designed to reproduce the surface using an interpolation function. 74 vertical and horizontal profiles were chosen within the impact area on which roughness parameters were calculated, separately, based on ISO 4287 standard [23]. Finally, all the calculated data were averaged to obtain the mean roughness parameters.

3. Experimental residual stress and surface roughness measurement

A series of residual stress measurements were carried out in parallel over the surface of the gears. The extraction of the residual stress data was performed by using the X-Ray Diffractometry (XRD) technique, which was applied to a local geometry. The gears were prepared by sectioning and installing portions of them over a holding device. The used instrument was a Stresstech Xstress 3000 G3 and the measurements were performed by applying the modified Chi method. A characteristic X-ray tube source of Cr was selected by using a round collimator and phi-rotational angle of 90°. The (hkl) 211 reflection crystallographic plane was selected for the collection with two detectors positioned at a distance of 50 mm from the sample at a diffraction angle of 156°. All measurements were performed following the guidelines as per Standard EN15305 [24]. Multiple points were tracked and the measurements at each point started with a surface measurement followed by material removing at several depths under the surface. A Young's modulus of 201 GPa and a Poisson's ratio of 0.29 were considered for the base material to estimate the macroscopic stress based on the diffraction peaks.

The surface roughness of the gear in the flank area was evaluated by means of a Mahr Perthometer equipped with a MFW-250 probe. The sampling and measurement procedures, including the selection of cut-off length and filtering techniques, were based on the ISO 4287 standard [23]. Based on the final product specification provided by the manufacturer, surface roughness parameters of the arithmetic mean (R_a) and the maximum profile height in the sampling length (R_z) were considered for further analysis.

4. Results

4.1. Material plasticity obtained by inverse analysis

Fig. 6 shows the final output for the performed inverse analysis. Fig. 6a and b present the comparison between inverse analysis and experimental indentation curves for the core and the carburized steel, respectively.

A perfect match is obtained for the core material, confirming the robustness of the procedure applied for the inverse analysis, including the developed optimization code. Fig. 6c and d illustrate the stress-strain responses for the core and the carburized steel, respectively, obtained by inverse analysis. For the core material (Fig. 6c), a proper agreement is observed between the experimental and calculated stress-strain response, which further validates the applied inverse analysis procedure. In Fig. 6d, the calculated stress-strain curve for each layer in the case region is depicted. As expected, with increasing hardness over the case, the stress-strain curve rises to higher stresses at constant strain values.

4.2. Single impact simulation

The results of the single-impact simulation are depicted in Fig. 7. A typical indent profile for a single impact analysis for an average impact angle of 17.5° is depicted in Fig. 7a.

The indent size was taken to be the distance between the points with vertical displacement equal to zero. As expected, the diameter of the indent varied by varying the impact direction; the outline of indents by a shot impact angle smaller than 90° tended to be elliptical, as confirmed by Kirk [25] and Ghelichi et al. [26]. For coverage calculations, the mean indent diameter was considered. It was calculated by averaging the semi-major (d_1) and minor axes (d_3) in directions 1 and 3 which are the main coordinate axes in the plane of the indent, as depicted in Fig. 7b. The results of the mean indent size as a function of impact angle for the single impact are shown in Table II. The data are provided for both of the utilized material models (hardness-based and inverse analysis). It is observed that the mean impact diameter decreases with decreasing impact angle, in accordance with a decline in the overall induced deformation.

4.3. Residual stresses

A typical contour plot of the Mises stress for 200% coverage after stage 1 is shown in Fig. 4d. The stresses are normalized by the ultimate tensile strength of the material. The numerical and

experimental residual stress profiles for stages 1 and 2 of multiple-impact SP with 200% coverage are shown in Fig. 8. The uncertainty of experimental data and subsequent error bars are such low that is not included in the relevant graphs. The numerical values were averaged over the impact area to simulate the averaging behavior of XRD stress measurement. The numerical results are depicted from different modeling approaches for the shot kinetics with material properties of the hardness-based method and inverse analysis. Different shot kinetics were implemented for the model with hardness-based material data. Based on the results of these first set of analysis, varying impact angle strategy was also considered for the model using material data obtained from the inverse-analysis method. The results of the analysis in which the mean impact angle was assigned to all shots is represented by "17.5°" label while varying impact angle approaches with a step size of 12.5° and 5° are shown by "30°-17.5°-5°" and "35°-0°:5°" labels, respectively. The later sequence consisted of angles 35°, 30°, 25°, 20°, 15°, 10°, and 5°. Fig. 8a represents the residual stresses after stage 1 of shot peening. At first glance, a reasonably good agreement is observed between the experimental and numerical results of all the performed analyses; the stresses start to grow into more compressive stresses just under the surface, passing through a maximum, after which they level off to less compressive values.

Regarding the models using hardness-based material data, the constant mean angle approach (17.5°), although depicting relatively favorable accordance with experimental data, deviates to a larger extent from the results of varying angle approaches. The varying angle approach, both with hardness-based and inverse analysis material data, exhibits the best match among all the analyses with the experimentation through the measured depth.

The numerical and experimental residual stress profiles for stage 2 with 200% coverage are shown in Fig. 8b. The numerical results are based on both material data sets with a varying impact angle of 12.5°. As it is observed, the numerical results are following the same trend as

the experimental ones, but compared to stage-1, the match is slightly less evident, especially from a depth of 0.05 mm to 0.20 mm when the maximum stress is passed. However, the data match between numerical and experimental results is still very good at depths immediately below the surface. The two material data sets are providing relatively identical results except for interior sections over which the inverse analysis material data is anticipating higher tensile stresses.

To further exhibit the importance of considering shot kinetics in terms of shot impact angle, the results of numerical residual stresses by assigning a normal impact angle to all shots, i.e., 90° is compared with the varying impact angle results as well as the experimental data in Fig. 9. It is observed that the consideration of a normal direction to all shots predicts much higher and deeper compressive residual stresses with larger compressive peak stress (~ 20%) and subsequently larger positive stresses in the interior sections with respect to the varying impact angle approach and the relevant experimental data.

4.4. Surface roughness

The experimental data of surface roughness, as well as the corresponding numerical results obtained by various modeling approaches, are provided in Table III. For SP stage 1, the normal impact angle results in notably higher roughness than the experimental one (four times for R_a and twice for R_z). However, the reduced impact angle approaches show improved results. It is observed that the mean angle approach is providing a perfect prediction for R_a parameter but lower estimation for the R_z parameter. Instead, the varying angle approaches, are exhibiting comparatively favorable results for both R_a and R_z parameters. With SP stage 2, the simulations were performed considering the varying impact angle approaches. Similar to stage 1, relatively favorable results are obtained for SP stage 2 compared to the corresponding experimental data. The variation of numerical roughness data is discussed further in the discussion section.

5. Discussion

In these sets of analyses, the numerical simulation of SP process on case-hardened gear was developed implementing the effect of the complex geometrical features of the gear and the gradient material properties. To consider the effect of geometry, the relative angle between the shot stream and the target shape was estimated based on the extension of the flow stream and the geometrical aspects of the gear tooth. In this regard, different strategies were considered to gradually vary the impact angle of the subsequent shots to take into account the effect of gear rotation during the SP process.

Gariépy et al. [27] explored the effect of velocity distribution in the shot stream by using finite element simulations and found that the depth of compressive residual stresses was affected by the velocity scatter. They proposed that consideration of velocity distribution especially the higher velocity impacts could lead to more actual SP predictions. Similar to this, the incorporation of varying impact angles into the modeling (with a step size of either 12.5° or 5°) compared to the fixed average angle was found to be beneficial in terms of the prediction of induced residual stresses on the flank area of the shot peened gear tooth. Higher angles of impact have higher velocities. This can be explained by the introduction of stronger high angle impacts, i.e., larger than the mean impact angle. The importance of high impact angles is especially noticed at depths lower than 0.12 mm (Fig. 8a). At stage I, decreasing the impact angle variation step size from 12.5° to 5° shows some improvements in the predictions of the model in the interior regions. However, it should be considered that as the step size decreases, the computational cost increases for very small angle impacts due to the longer contact durations. Considering the relatively large number of impacts, especially at high coverage levels (200%-400%), this could be an issue and the selection of the proper step size should be accomplished with a compromise between the simulation accuracy and the computational cost. The varying impact angle approaches seem to be capable of predicting maximum compressive residual stress occurring at a depth of around 0.05 mm with higher accuracy. However, beyond

0.12 mm, the capability of the model to predict the stresses is independent of the impact angle setting.

To examine further the validity of the methods implemented to consider the gradient variation of material properties in-depth, the stress-strain responses for the first and second top layers of the case, i.e. L1 and L2 Fig. 2b, two material data sets obtained by the hardness-based approach and inverse analysis approach, are plotted together in Fig. 10. The top layers are the most influential ones on the plasticity and subsequent induced stresses and surface roughness. It is observed that the predicted plastic behavior by the inverse analysis method is always above the expected response by the hardness method. The strength dissimilarity between the two approaches is about 12% at a plastic strain of 0.1, which is not a huge difference. Therefore, the two material model outputs in terms of the single indent size (Table II) and the induced residual stresses (Fig. 8) were expected to be not so dissimilar, which turns out to be true. Although the hardness approach is more simplistic than the inverse analysis method, it is still able to provide sufficiently satisfactory residual stress predictions compared to the more complex inverse analysis approach.

The probable source for the observed discrepancy between the numerical and experimental residual stress data in stage 2 (Fig. 8b) could be the lower accuracy of extrapolated material data at high plastic strains using the corresponding material model. Upon SP stage 2, a total of 400% SP coverage is applied to the material, which indicates very large plastic deformations induced at the topmost surface. Extrapolation of low strain material data to larger plastic strains may result in inaccuracy in the simulations. It is a common finding that with severe plastic deformation, microstructural alteration and/or grain refinement occurs, which may modify the material behavior [28]. This, in turn, can modify the subsequent induced residual stresses by stress relaxation [29]. To overcome this problem, researchers try to develop phenomenological material constitutive models [30].

Similar to the effect observed in residual stresses (Fig. 9), relatively large deviations in surface roughness parameters with normal impacts prove further that adapting shot kinetics and impact angles to the geometry of the shot peened part is essential for the accuracy of the simulations. For SP stage 1 in the mean impact angle approach, an excellent prediction of the R_a parameter is obtained, but lower R_z value is predicted. This could be due to the exclusion of high and low impact angles. It is observed that the incorporation of such impacts in the varying impact angle approaches improves the predicted value for the R_z parameter. Besides, it is noticed that regarding the varying angle approaches in stage 1, the highest roughness values are obtained with a 5° step. This turns out to be the reverse of what is obtained for the residual stresses, which show improved results in case of smaller step size. However, attention is drawn to the imbalance of applied angles in the 5° step approach; the high impact angles ($30° < \theta \leq 35°$) are included in the model but the equivalent low impacts ($0° < \theta < 5°$) are not. Although the effects of low impact angles are negligible on the residual stresses, they could have a considerable effect on the surface roughness since low impact angles are expected to have a smoothening action, which reduces the height of the surface peaks.

Roughness parameters of stage 1 predicted from the model using inverse analysis material data are lower than the ones obtained from the hardness-based material model. This seems to agree with the previous discussion on the higher strength of inverse analysis material data. Higher strengths would lead to lower plastic deformations and reduced roughness.

Dual peening is a modified version of the conventional shot peening process in which the SP treatment is performed in two steps to increase the homogeneity of the stresses and surface morphology [31]. In recent years, multistep SP has attracted more attention. Multistep SP with proper intensities has been shown to be an operative method for the optimization of the residual stresses and microstructure of 18CrNiMo7-6 steel [32]. Later, the beneficial effects of multistep SP were proved for GCr15 steel [33]. In terms of roughness, it is observed that the

application of SP stage 2 imposes a slight modification of the experimental roughness parameters. While the magnitude and depth of stresses are not affected much with the application of stage 2 (Fig. 8). There is a slight reduction of experimental roughness parameters after the second peening stage. The roughness parameters obtained from the numerical model also slightly decreased after stage 2 regardless of the varying angle approach or material. This is in agreement with the decrease in the experimental R_z parameter.

6. Conclusions

A detailed numerical model of the dual air-blast shot peening process applied to a case-hardened gear was developed. Two different approaches were implemented to incorporate the effect of the in-depth gradual variation of material properties for carburized steel. One method was based on the local microhardness variations in the depth of the hardened case and the other used an inverse analysis approach to estimate the layer by layer variation of material properties. Experimental indentation tests were conducted to capture the response of the material in the latter approach. The effect of the complex gear tooth geometry was incorporated by gradually altering the impact direction of successive shots, to simulate the variation of impact direction with respect to the tooth flank as the gear was rotated under the shot stream during the experimental shot peening treatment. The obtained results indicated that

- Both the hardness-based material model and the inverse analysis material model are capable of providing a proper estimation of the case-hardened material response under multiple impacts of the shot peening treatment in terms of residual stresses. Considering the simplicity of the hardness-based method, it can be selected as a more convenient choice for estimating the distribution of residual stresses in shot peened case-hardened steels.
- Considering the effect of the gear tooth geometry, the distribution of residual stresses obtained for multiple impact models using varying impact angles exhibited good

agreement with the experimental XRD data in the first stage of shot peening. This observation highlights the importance of taking the real distribution of impact angles during the shot peening treatment into account. For the second stage of shot peening, residual stresses were not fully captured by the model, most probably because of the less accurate material data estimated at high plastic strains.

- Surface roughness parameters calculated based on the displacement results of the simulations showed proper agreement with the experimental data. The surface roughness results for the second stage provided an even better agreement with the experimental data.

Overall, the results confirm the efficiency of the developed model in providing a good estimation of the distribution of the residual stresses and surface roughness induced by dual shot peening on carburized steels. This study highlights the importance of considering realistic assumptions regarding target geometry and material properties in the simulation of impact-based mechanical surface treatments, especially when applied to mechanical components with complex geometry and with graded material surface properties.

Acknowledgments

The investigations were conducted as part of a research program funded by Aerospace Transmission Technologies GmbH, supported by Rolls-Royce Deutschland Ltd & Co KG.

Data availability

The detailed raw/processed data required to reproduce these findings cannot be shared at this time to preserve confidentiality.

References

[1] M. Widmark, A. Melander, Effect of material, heat treatment, grinding and shot peening on contact fatigue life of carburised steels, Int. J. Fatigue 21 (1999) 309-327.

[2] M. Benedetti, V. Fontanari, B.R. Höhn, P. Oster, T. Tobie, Influence of shot peening on bending tooth fatigue limit of case hardened gears, Int. J. Fatigue 24 (2002) 1127-1136.

[3] M. Guagliano, E. Riva, M. Guidetti, Contact fatigue failure analysis of shot-peened gears, Eng. Failure Anal. 9 (2002) 147-158.

[4] M.D. Lawerenz, Shot peening and its Effect on Gearing, SAE Technical Paper, 1984.

[5] S.A. Meguid, G. Shagal, J.C. Stranart, J. Daly, Three-dimensional dynamic finite element analysis of shot-peening induced residual stresses, Finite Elem. Anal. Des. 31 (1999) 179-191.

[6] S.T.S. Al-Hassani, K. Kormi, D.C. Webb, in: A. Nakonieczny (Ed.) Proceedings of the 7th International Conference on Shot Peening, Warsaw, Poland, 1999, pp. 217–227.

[7] M. Guagliano, Relating Almen intensity to residual stresses induced by shot peening: a numerical approach, J. Mater. Process. Technol. 110 (2001) 277-286.

[8] X. Kang, T. Wang, J. Platts, Multiple impact modelling for shot peening and peen forming, Proc. Inst. Mech. Eng. B 224 (2010) 689-697.

[9] T. Kim, J.H. Lee, H. Lee, S.-k. Cheong, An area-average approach to peening residual stress under multi-impacts using a three-dimensional symmetry-cell finite element model with plastic shots, Mater. Des. 31 (2010) 50-59.

[10] S. Bagherifard, R. Ghelichi, M. Guagliano, On the shot peening surface coverage and its assessment by means of finite element simulation: A critical review and some original developments, Appl. Surf. Sci. 259 (2012) 186-194.

[11] H.Y. Miao, S. Larose, C. Perron, M. Lévesque, On the potential applications of a 3D random finite element model for the simulation of shot peening, Adv. Eng. Softw. 40 (2009) 1023-1038.

[12] S. Bagherifard, R. Ghelichi, M. Guagliano, Mesh sensitivity assessment of shot peening finite element simulation aimed at surface grain refinement, Surf. Coat. Technol. 243 (2014) 58-64.

[13] D. Kirk, M. Abyaneh, Theoretical basis of shot peening coverage control, Shot Peener 9 (1995) 28-30.

[14] A. Heydari Astaraee, R. Miresmaeili, S. Bagherifard, M. Guagliano, M. Aliofkhazraei, Incorporating the principles of shot peening for a better understanding of surface mechanical attrition treatment (SMAT) by simulations and experiments, Mater. Des. 116 (2017) 365-373.

[15] F. Yang, Z. Chen, S.A. Meguid, Effect of initial surface finish on effectiveness of shot peening treatment using enhanced periodic cell model, Int. J. Mech. Mater. Des. (2014) 1-16.

[16] P. Sanjurjo, C. Rodríguez, I. Peñuelas, T.E. García, F.J. Belzunce, Influence of the target material constitutive model on the numerical simulation of a shot peening process, Surf. Coat. Technol. 258 (2014) 822-831.

[17] G. Donzella, A. Pola, L. Solazzi, G. Marconi, Effect of shot peening on carburised surfaces, Int. J. Mater. Prod. Tec. 15 (2000) 117-130.

[18] R. Pedersen, S. Rice, Case crushing of carburized and hardened gears, SAE Technical Paper, 1961.

[19] C. Moussa, O. Bartier, G. Mauvoisin, P. Pilvin, G. Delattre, Characterization of homogenous and plastically graded materials with spherical indentation and inverse analysis, J. Mater. Res. 27 (2012) 20-27.

[20] C. Moussa, O. Bartier, G. Mauvoisin, X. Hernot, J.-M. Collin, G. Delattre, Experimental and numerical investigation on carbonitrided steel characterization with spherical indentation, Surf. Coat. Technol. 258 (2014) 782-789.

[21] S. Bagherifard, R. Ghelichi, M. Guagliano, A numerical model of severe shot peening (SSP) to predict the generation of a nanostructured surface layer of material, Surf. Coat. Technol. 204 (2010) 4081-4090.

[22] S. Bagherifard, M.F. Molla, D. Kajanek, R. Donnini, B. Hadzima, M. Guagliano, Accelerated biodegradation and improved mechanical performance of pure iron through surface grain refinement, Acta Biomater. 98 (2019) 88-102.

[23] ISO Standard 4278: Geometrical Product Specifications (GPS) – Surface Texture: Profile Method Terms, Definitions and Surface Texture Parameters, International Organization for Standardization, Geneva, Switzerland, 1997.

[24] EN Standard 15305: Nondestructive Testing—Test Method for Residual Stress Analysis by X-Ray Diffraction, 2008.

[25] D. Kirk, Effects of Varying Shot Impact Angle, Shot Peener 19 (2005) 24-26.

[26] R. Ghelichi, G. Crispiatico, M. Guagliano, S. Bagherifard, An energetic approach to predict the effect of shot peening-based surface treatments, Met. 8 (2018) 190.

[27] A. Gariépy, H.Y. Miao, M. Lévesque, Simulation of the shot peening process with variable shot diameters and impacting velocities, Adv. Eng. Softw. 114 (2017) 121-133.

[28] O. Unal, R. Varol, Surface severe plastic deformation of AISI 304 via conventional shot peening, severe shot peening and repeening, Appl. Surf. Sci. 351 (2015) 289-295.

[29] R. Wawszczak, A. Baczmański, C. Braham, W. Seiler, M. Wróbel, K. Wierzbanowski, A. Lodini, Residual stress field in steel samples during plastic deformation and recovery processes, Philos. Mag. 91 (2011) 2263-2290.

[30] S. Amir H. Motaman, U. Prahl, Microstructural constitutive model for polycrystal viscoplasticity in cold and warm regimes based on continuum dislocation dynamics, J. Mech. Phys. Solids 122 (2019) 205-243.

[31] A. Ahmad, E. Crouch Jr, Dual shot peening to maximize beneficial residual stresses in carburized steels, Shot Peener 16 (2002) 7-10.

[32] P. Fu, K. Zhan, C. Jiang, Micro-structure and surface layer properties of 18CrNiMo7-6 steel after multistep shot peening, Mater. Des. 51 (2013) 309-314.

[33] P. Fu, C. Jiang, Z. Zhang, V. Ji, Residual stress and micro-structure of GCr15 steel after multistep shot peening, Surf. Eng. 30 (2014) 847-851.

Table I SP process parameters for dual shot peening of gear

SP stage	Media	Almen intensity	Coverage %	Velocity m/s
1	Ceramic 1	10A	200	38.6
2	Ceramic 2	16A	200	42.0

Table II Mean dimple diameter of a single impact

Impact angle (°)	90	35	30	25	20	15	10	5
Diameter by hardness-based material data (mm)	0.186	0.142	0.131	0.122	0.115	0.109	0.095	0.085
Diameter by inverse analysis material data (mm)	0.179	0.140	0.131	0.121	0.111	0.104	0.094	0.081

Table III Experimental (exp.) and numerical (num.) surface roughness parameters after stages 1 and 2 of SP based on the hardness-based (H) and inverse analysis (IA) material models

SP stage	stage 1		stage 2	
Roughness parameter, μm	R_a	R_z	R_a	R_z
Exp.	0.61	4.98	0.64	4.67
90° (H)	2.57	10.87	-	-
17.5° (H)	0.62	3.50	-	-
30°-17.5°-5° (H)	0.73	4.49	0.62	4.11
30°-17.5°-5° (IA)	0.65	4.38	0.60	4.04
35° - 0°: 5° (H)	0.90	5.03	0.78	4.16

Fig. 1 Stress-strain curve of the gear steel core material

Fig. 2 a) Variation of the Vickers microhardness profile of the carburized steel in the flank region as a function of depth below the surface b) Definition of the layered model for the carburized steel.

Fig. 3 a) Experimental setup for indentation testing using a tensile test machine, b) details of designed support for the indenter

Fig. 4 a) The numerical model of the spherical indentation test with mesh details used in inverse analysis b) geometry of the 3D numerical model of single and multiple impact SP c) mesh details of the impact area in (b) d) Von-Mises stress contour after stage 1 with 200% SP coverage, normalized by the ultimate tensile strength of the material.

Fig. 5 a) Characteristics of the shot stream b) arrangement of gear under the shot stream in constant intensity zone and the estimated maximum impact angle

Fig. 6 Comparison between the inverse analysis and experimental indentation curves for a) the core material b) the top surface of the carburized steel c) comparison between inverse analysis and experimental stress-strain curve for the core material d) inverse analysis results for stress-strain curves of the case layers.

Fig. 7 Vertical displacement at indent centerlines in directions 1 and 3 with an impact angle of 17.5°, using hardness-based material data.

Fig. 8 Comparison between numerical and experimental residual stresses after a) SP-stage 1 b) SP-stage 2, based on the hardness-based (H) and inverse analysis (IA) material models.

Fig. 9 Comparison of numerical residual stresses after SP stage 1 considering the varying impact angle and normal impact angle approaches based on the hardness-based (H) material model

Fig. 10 Comparison of material plasticity data obtained by hardness-based (H) and inverse analysis (IA) approaches in the topmost layers L1 and L2

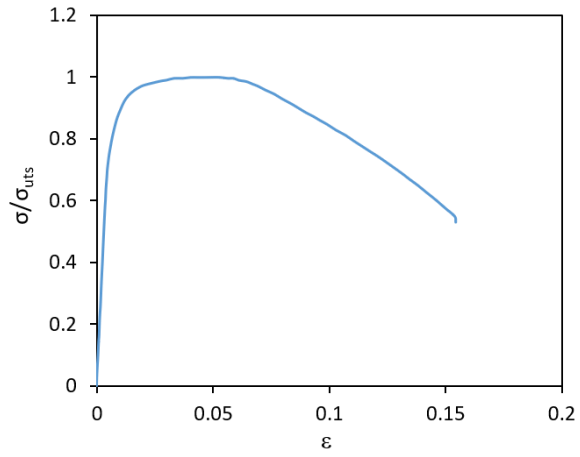

1

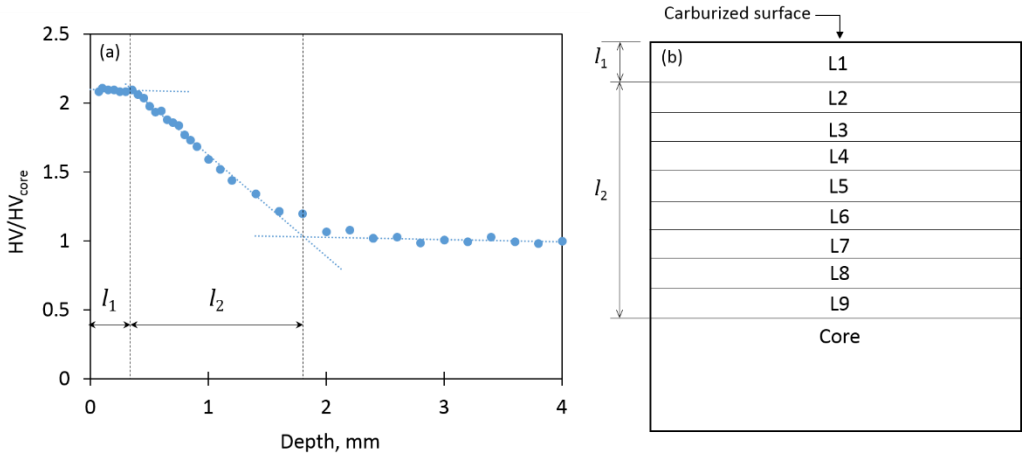
(a)
HV/HV$_{core}$
2.5
2
1.5
1
0.5
0
0
1
2
3
4
Depth, mm
l_1
l_2
Carburized surface
(b)
L1
L2
L3
L4
L5
L6
L7
L8
L9
Core

2

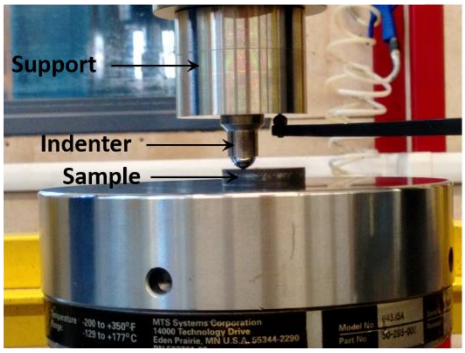
Support
Indenter
Sample
MTS Systems Corporation
14000 Technology Drive
Eden Prairie, MN U.S.A. 55344-2290

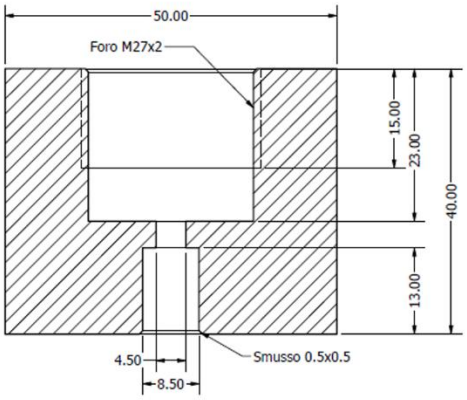
50.00
Foro M27x2
15.00
23.00
40.00
13.00
4.50
8.50
Smusso 0.5x0.5

3

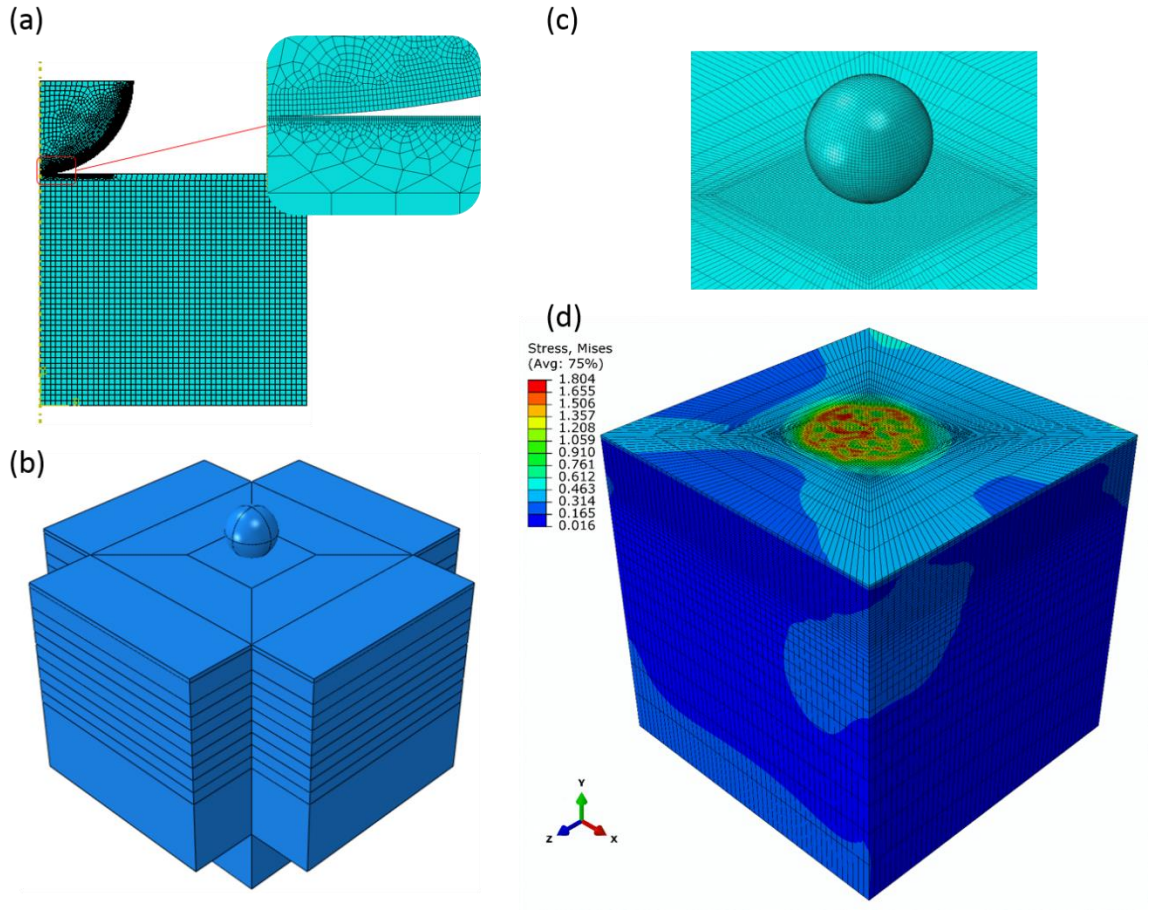
(a)
(b)
(c)
(d)
Stress, Mises
(Avg: 75%)
1.804
1.655
1.506
1.357
1.208
1.059
0.910
0.761
0.612
0.463
0.314
0.165
0.016
Y
z
x

4

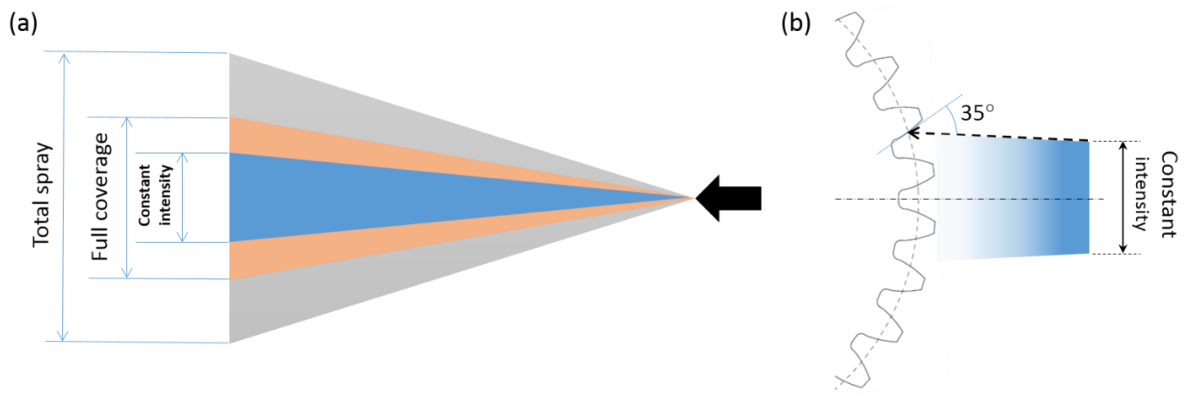
(a)
Total spray
Full coverage
Constant intensity
(b)
35°
Constant intensity

5

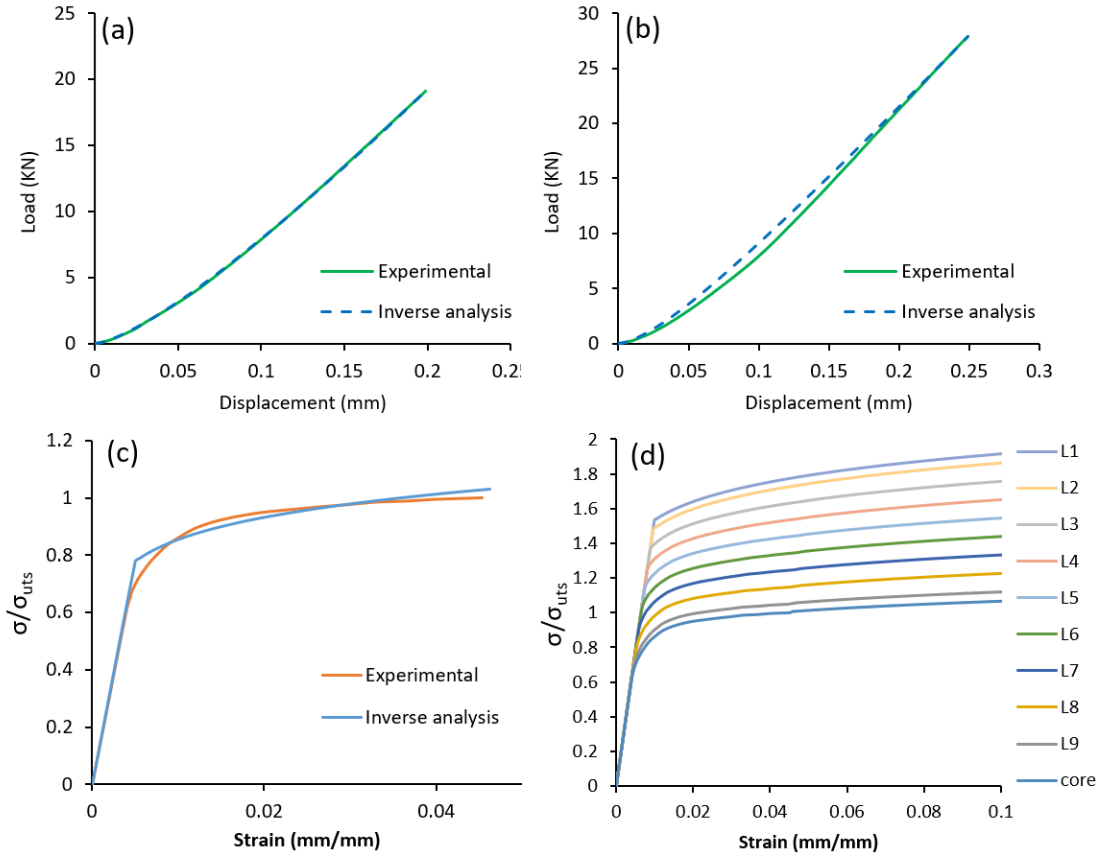
(a)
Load (KN)
Displacement (mm)
Experimental
Inverse analysis
(b)
Load (KN)
Displacement (mm)
Experimental
Inverse analysis
(c)
σ/σuts
Strain (mm/mm)
Experimental
Inverse analysis
(d)
σ/σuts
Strain (mm/mm)
L1
L2
L3
L4
L5
L6
L7
L8
L9
core

6

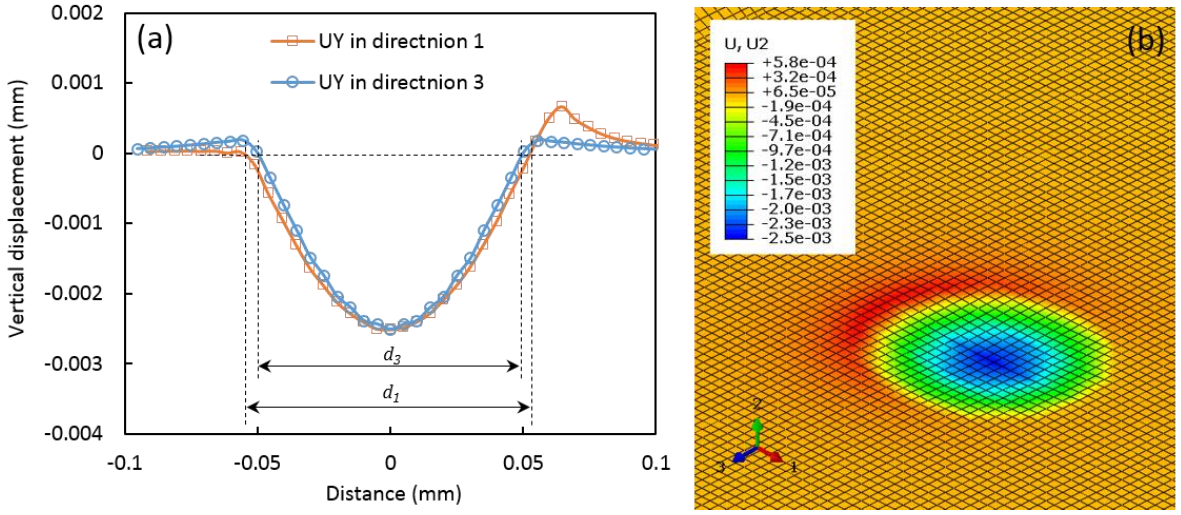
(a)
UY in directnion 1
UY in directnion 3
Vertical displacement (mm)
0.002
0.001
0
-0.001
-0.002
-0.003
-0.004
-0.1
-0.05
0
0.05
0.1
Distance (mm)
d_3
d_1
(b)
U, U2
+5.8e-04
+3.2e-04
+6.5e-05
-1.9e-04
-4.5e-04
-7.1e-04
-9.7e-04
-1.2e-03
-1.5e-03
-1.7e-03
-2.0e-03
-2.3e-03
-2.5e-03
2
3
1

7

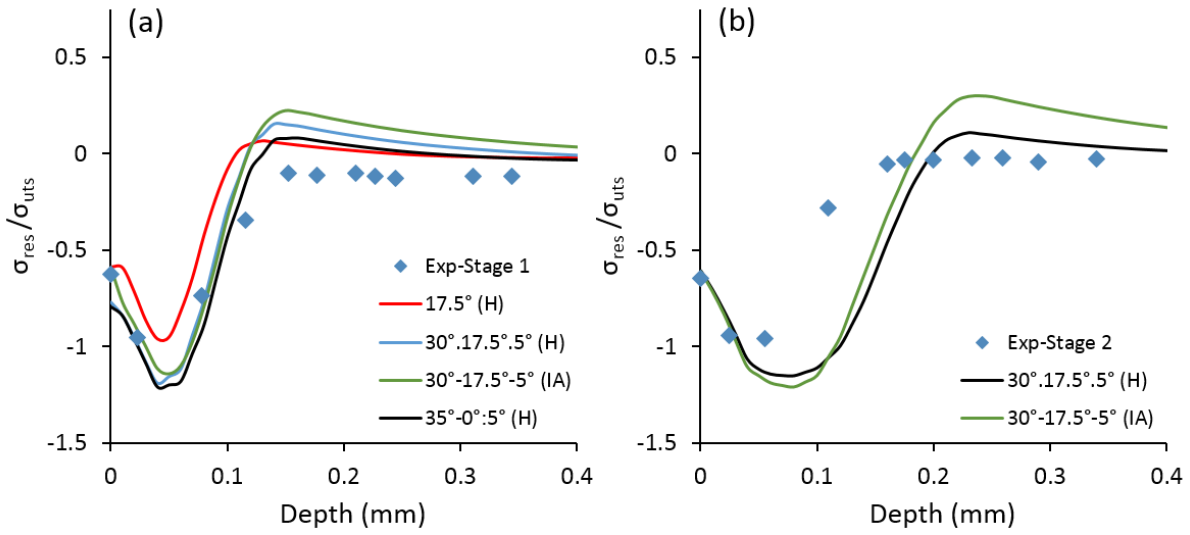
(a)
0.5
0
-0.5
-1
-1.5
σres /σuts
0
0.1
0.2
0.3
0.4
Depth (mm)
Exp-Stage 1
17.5° (H)
30°.17.5°.5° (H)
30°-17.5°-5° (IA)
35°-0°:5° (H)
(b)
0.5
0
-0.5
-1
-1.5
σres /σuts
0
0.1
0.2
0.3
0.4
Depth (mm)
Exp-Stage 2
30°.17.5°.5° (H)
30°-17.5°-5° (IA)

8

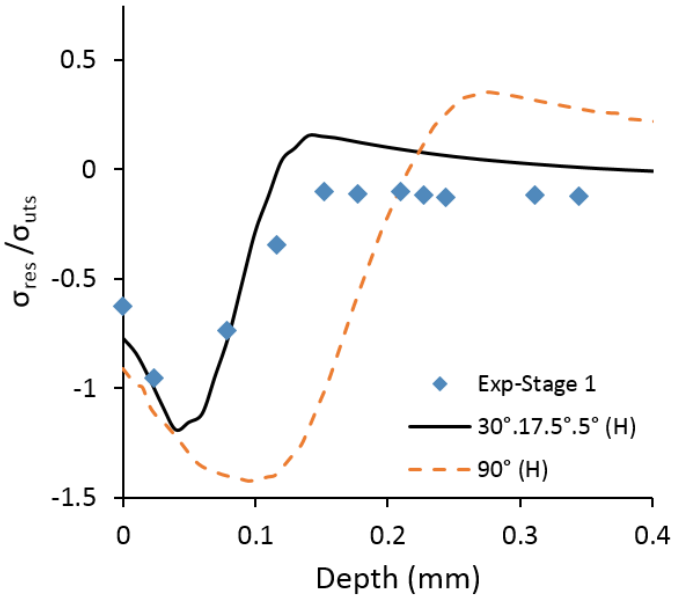
0.5
0
-0.5
-1
-1.5
0
0.1
0.2
0.3
0.4
Depth (mm)
σres /σuts
Exp-Stage 1
30°.17.5°.5° (H)
90° (H)

9

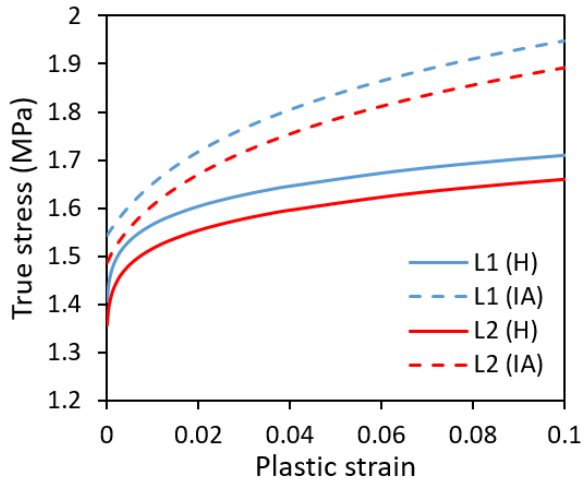
True stress (MPa)
2
1.9
1.8
1.7
1.6
1.5
1.4
1.3
1.2
0
0.02
0.04
0.06
0.08
0.1
Plastic strain
L1 (H)
L1 (IA)
L2 (H)
L2 (IA)

10